World Journal of Advanced Research and Reviews
eISSN: 2581-9615 CODEN (USA): WJARAI
Cross Ref DOI: 10.30574/wjarr
Journal homepage: https://wjarr.com/

(RESEARCH ARTICLE)

Check for updates

Computational Fluids Dynamics of air and water flows subjected to turbulence and confronted with cold fronts in a three-inlet-T-junction duct followed by two 90-degree elbows connected by a straight section of adjustable length (C-shaped elbow)

Pape Tamsir Ndiaye [1,*], Goumbo Ndiaye [2], Momath Ndiaye [1,3], Oumar Drame [1,4] and Omar Ngor Thiam [1,4]

[1] *Fluid Mechanics and Transfer Laboratory, Department of Physics, Sciences and Technologies Faculty, Cheikh Anta DIOP University, Dakar-Fann, Senegal.*
[2] *The Water, Energy, Environment and Industrial Processes Laboratory of the Polytech Higher School, Cheikh Anta Diop University, Dakar, Senegal*
[3] *Department of the Ufr Hydraulics, Rural Engineering, Machinery and Renewable Energy,University of Sine Saloum Elhadji Ibrahima NIASS, Kaolack, Senegal.*
[4] *Research Group on Solar Energy and Transfers (GREST), Sciences and Technologies Faculty, Cheikh Anta DIOP University, Dakar-Fann, Senegal.*

World Journal of Advanced Research and Reviews, 2025, 27(02), 693-705

Publication history: Received on 30 June 2025; revised on 09 August 2025; accepted on 11 August 2025

Article DOI: https://doi.org/10.30574/wjarr.2025.27.2.2839

Abstract

This study examines air and water flows in a three-inlet T-junction duct followed by two 90° elbows connected by a straight section of adjustable length (C-shaped elbow), with a particular focus on the impact of the straight section length between the two 90° elbows. The analysis focuses on the behavior of the fluids (air and water) along the duct axis (x, y, z=0), after the mixing zone (at 70 mm), upstream of the first elbow, and at the duct outlet. The numerical solution is based on the realizable k-Ɛ viscous turbulence model coupled with the energy equation, implemented in Ansys Fluent 2024R2. Three straight section length cases were studied: Case I (L= 20 mm), Case II (L=50 mm), and Case III (L=100 mm). According to the results obtained, the c-bend, consisting of two 90° elbows connected by the straight section, intensifies the turbulence within the flow, with effects depending on the thermophysical characteristics of the fluid (density, thermal conductivity, kinematic viscosity, etc.). The straight section connecting the two 90° elbows moderates the combined dynamic and thermal disturbances of the successive elbows. If it is too short, it aggravates the disturbances; if properly dimensioned, it acts as a stabilizing buffer zone, improving the thermal and hydraulic efficiency of the duct.

Keywords: Ansys Fluent; Air and water movement; C-elbow; CFD; Heat and mass transfer; realizable k-ε turbulence model; Straight section; T-Junction;

1. Introduction

Mixing air at different temperatures is essential to ensure optimal thermal comfort and satisfactory indoor air quality. In the fields of heating, ventilation, and air conditioning (HVAC), controlling the movement and interactions between hot and cold air flows is essential. Similarly, mixing water at different temperatures is important in the design of wastewater treatment plants, water treatment systems, sanitation networks, and hydraulic engineering. The geometry of ducts (tubes, channels, conduits, channels, and vents, etc.) strongly influences the flow dynamics of both air and water to achieve acceptable quality. In piping networks, T- or Y-type junctions are commonly used to distribute or collect flows. These junctions, along with other elements such as valves, turbines, pumps, elbows, elbow-junctions, contractions, expansions, meters introduce major as well as minor pressure losses, affecting the overall efficiency of the

* Corresponding author: Pape Tamsir Ndiaye

systems. Many experimental and numerical research works with tools such as Ansys Fluent, OpenFOAM have been carried out to better understand this phenomenon [1-16].

A multiphase flow model through the T-junction and the phase redistribution phenomenon at the junction using ANSYS FLUENT software was presented by Athulya A. Sa et al. [1]. The following conclusions were drawn based on their study: a larger amount of air pocket is formed in the lower part of the bypass arm, phase separation is negligible in the bypass arm due to the effect of gravity and by analyzing the multiphase flow, they found that considering the fluid alone, the phase separation is greater at the outlet than at the junction.

Nimadge Mr.G.B. et al. [2] aimed to study the steady and incompressible flow of a fluid through a T-junction and to get familiar with CFD focusing on losses in piping systems, as the working fluid through pipes plays an important role in the operation of industries such as chemical industries, petroleum industries, etc. They started with an experimental setup to obtain reference data as the fluid passes through the pipe T-junction, and then the same data were used for CFD analysis using software such as ANSYS FLUENT.

Khan Wasim et al. [3] conducted a numerical study on the mechanism of plug formation during two-phase gas-liquid flow in a T-junction microchannel. They developed a two-dimensional (2D) model of the microchannel using ANSYS Academic Research CFD 18.2 software and the volume of fluid (VOF) method to solve it. Their results showed good agreement with the experimental data. They measured the plug length, pressure drop, and velocity variations inside the plugs for different operating conditions. The study also investigated the influence of contact angle (0°–155°), fluid viscosity, and surface tension on the two-phase flow interaction parameters, as well as the effect of gas and liquid superficial velocities. They found that at low capillary number (Ca), the liquid film formed was very thin, observable only with fine meshes near the channel walls.

DOROSHENKO Yaroslav et al. [4] performed 3D modeling of the elbow and T-junction located in the linear part of a gas pipeline, especially in areas where the multiphase flow adopts complex trajectories and changes direction. Based on the Lagrangian approach (Discrete Phase Model - DPM), they developed numerical modeling methods to model the behavior of multiphase flow in these structures, using ANSYS FLUENT R17.0 Academic software. The mathematical model is based on the solution of the Navier-Stokes equations and the discrete phase continuity and motion equations, coupled with the Launder-Sharma k-Ɛ turbulence model, with suitable initial and boundary conditions. The results obtained allow a thorough and comprehensive analysis of the erosive wear of the elbow and T-junction of the linear part of the gas pipeline and adjacent sections of the pipeline, as well as an assessment of their strength and residual service life. The velocities of liquid and solid particles, impact angles, diameters of condensed droplets and solid particles at the collision site were determined. This work paves the way for a better understanding of erosive wear phenomena in gas pipelines.

RAID AHMED MAHMOOD [5] conducted a CFD simulation to predict and visualize the separation of two-phase flows in the vertical T-junction. A comparison between the CFD results and the associated experimental data was carried out to validate the simulations. For this purpose ANSYS 17.1 was used for the numerical simulation, with a geometry of the T-junction designed via the ANSYS design module, based on the dimensions of the experimental section, then meshed using ANSYS Meshing to obtain a suitable mesh. Furthermore Chiriac Eugen et al. [6] conducted a numerical study of a three-inlet Y-junction microchannel, using two separate software ANSYS Fluent and Open-FOAM, under identical inlet and boundary conditions. Three main parameters are studied: velocity amplitude, pressure and vorticity amplitude. The microchannel was fabricated by soft litography in PDMS (Polydimethylsiloxane) and was used for the validation of numerical simulations. The microchannel was fabricated using PDMS (Polydimethylsiloxane) soft litography and used to validate numerical simulations. A comparison of the simulation results allowed evaluating the respective performances of the two numerical codes in modeling flow mixing in a microchannel.

Makarem M. A. [7] performed a CFD simulation to study CO2 capture in a microchannel by aqueous mixtures of MEA and [Bmim] BF4 modified with TiO2 nanoparticles as chemical additives. Their work focuses on the hydrodynamic analysis of flow, mass transfer and CO_2 absorption performance in a T-shaped microchannel geometry, in a steady state of the computational fluid dynamics technique. Their models are based on the Navier-Stokes and continuity equations coupled with a laminar model with mass transfer between heterogeneous phases. They examined the influence of mass fractions of [Bmim] BF_4 (up to 10%) and TiO_2 (up to 0.1%) on CO_2 loading, bubble formation and velocity distribution under various gas-liquid retentions. Their results indicate that the optimal composition (10% [Bmim] BF_4, 3% MEA, 0.04% TiO_2) allowed to achieve a maximum purification rate of 79.62%.

Taha Enas Salman et al. [8] explored the impact of turbulent parameters on the characteristic centerline of a fluid flow through a T-junction connected to a Venturi tube via a pipe. Using ANSYS FLUENT 2020R1 and the standard k-ε

turbulence model, they solved the continuity, momentum, and energy equations. They analyzed the velocity distribution and pressure drops, turbulent kinetic energy, and dissipation. The results revealed a marked divergence in velocity and pressure drops, while they showed similar behavior for the turbulence parameters.

SAID Mohammed et al. [9] conducted a 3D numerical simulation of liquid/liquid two-phase flow in a rectangular microchannel with a T-junction, using the volume of fluid (VOF) method with ANSYS Fluent, combined with adaptive meshing and a symmetry assumption to optimize the calculation. They identified six distinct flow patterns by dispersing water in a continuous silicone oil phase. Reducing the flow rate ratios as well as the viscosity leads to an increase in the liquid film thickness in the corners and side planes, which significantly affects the film and plug velocities.

Bushra Khatoon et al. [10] proposed a numerical simulation and experiment to analyze the hydrodynamics and mass transfer in a crossed T-junction microchannel subjected to a gas-liquid flow system. The CO2-water hydrodynamic simulation via ANSYS-FLUENT 2021 R2 with the fluid volume technique was validated by experimental data. They observed that the total volumetric mass transfer coefficient (margin 0.1–0.8 1/s) increases with gas velocity, but decreases with film thickness (0.01–0.05 mm) and temperature (T = 298.15 K and 303.15 K). An increase in bubble velocity also increases this coefficient, unlike film thickening, due to the dominant effect of surface tension.

Wang Fuzhang et al. [11] studied the dynamics of unsteady air and water in a three-inlet T-shaped duct, focusing on the formation of cold fronts. Using the k-ε viscous model developed under Ansys Fluent 2022R1, they examined the flow evolution before and after the bend. Three inlet velocity configurations were tested. Verification of the convergence of the results was ensured by performing residual and mesh independence analysis. Three cold front formation configurations were studied according to the variations of the inlet velocity. When the inlet velocities of cold air/water and hot air/water were equal, no cold front was noticeable at the early stages, although the air velocity remained higher than that of the water. The authors observed that the maximum average kinetic energy of the vortices per unit mass developed mainly near the T-junction, not as a direct result of the previously formed cold fronts, but due to the recirculation of the pressure generated at the elbow, influencing the velocity of the cold flows coming from the two vertical inlets (inlet 2 and inlet 3).

However, similarly to Wang Fuzhang et al. [11], we propose a CFD numerical study and a comparative study between the dynamics of air and water through a three-inlet T-junction duct followed by two 90° elbows connected by a straight section of adjustable length (C-shaped elbow). We will study the influence of the variation of the length of the straight section connecting the two 90° elbows on the flow and the overall dynamics, in particular the velocity field, pressure and temperature variations and turbulence, as well as how they vary in the duct at a distance after mixing, before the elbows and after the elbows. We will also study the impact of these parameters on the formation and behavior of cold fronts, highlighting the differences in behavior between air and water.

2. Mathematical Formulation

2.1. Description of the physical model and simplifying assumptions:

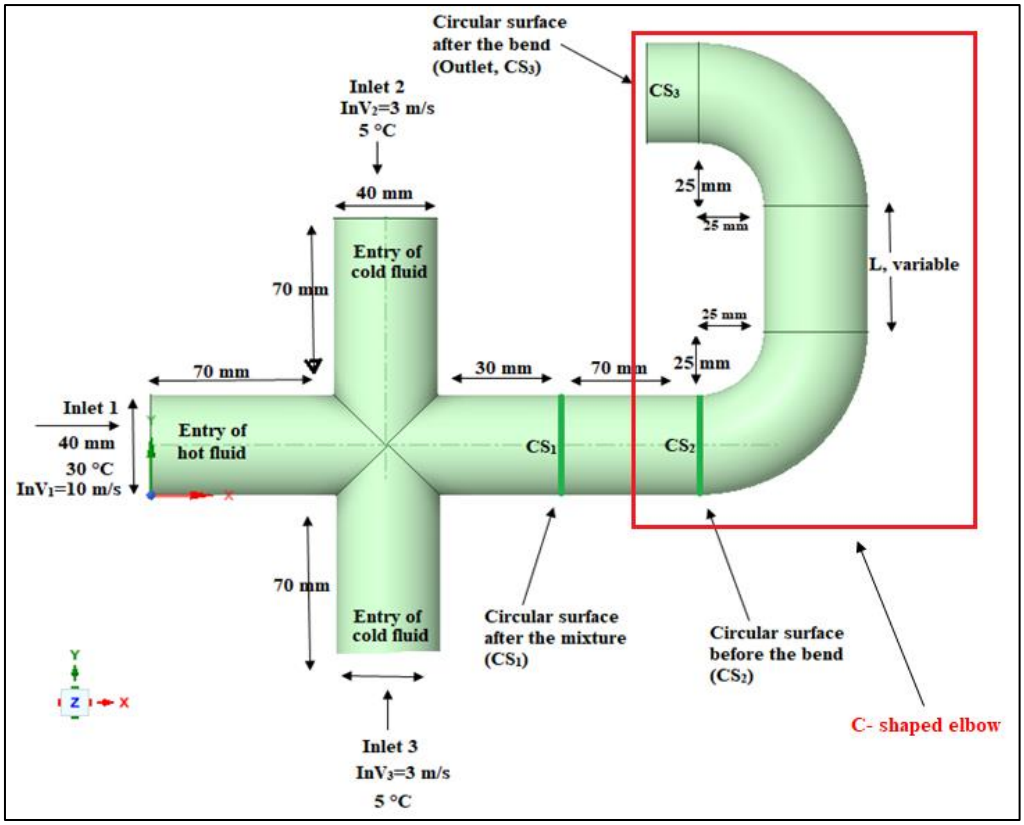

Figure 1 Illustration of the geometric model (a three-inlet-T-junction duct followed by two 90-degree elbows connected by a straight section of adjustable length (C-shaped elbow))

In this study, we consider two circular aluminum ducts of 40 mm diameter, where it is assumed that air and water flow separately in each of the ducts in the form of a T-junction with three inlets followed by two 90° elbows connected by a straight section of adjustable length (C-shaped elbow). As shown in Figure 1, the mixing zone is located 70 mm from inlets 1, 2 and 3 in each of these ducts. The geometric configuration in 3D mode includes a first circular surface (CS1) located 30 mm from the mixing zone, a second circular surface (CS2) located 100 mm from the same zone, just before the first elbow and an outlet surface located 20 mm from the second elbow of the duct (CS3). The hot fluid (air or water) enters the domain through inlet 1 with a speed InV1 = 10 m/s and a temperature of 30 °C, on the other hand the cold fluid inlets are found through inlets 2 and 3 with respectively speeds InV2 = InV3 = 3 m/s at 5 °C, which will favor cold fronts according to Wang Fuzhang et al. [11], The low speed of the cold fluid (air and water) at inlets 2 and 3 and a high speed at inlet 1 generates an extended cold front. The physical properties of the fluids are summarized in Table 1.

Table 1 The physical properties of the fluid considered: air and liquid water

	Air	**liquid water**
Density ρ : [Kg/m^3]	1.225	998.2
Viscosity μ : [Kg/(m.s)]	1.7894-× 10^{-5}	1.003× 10^{-3}
Thermal Conductivity k : [W/(m.K)]	0.0242	0.6
Specific Heat Cp : [J/(Kg.K]	1006.43	4182

To carry out this work well, we consider certain simplifying assumptions such as: fluids (water and air) are considered incompressible and Newtonian, quasi-constant physical properties, no phase change and fully turbulent and permanent flow.

2.2. Governing equations:

Given that Reynolds Averaged Navier-Stokes (RANS) models have certain limitations, they deserve to be recognized as among the most reliable for characterizing the velocity fields of turbulent flows due to their near-wall modeling. Turbulence modeling (i.e., involving the averaging of the equations governing fluid motion over time or space to obtain a mean flow field and additional terms representing turbulence effects), reliable for higher Reynolds numbers, inherently assumes that turbulent fluctuations can be decomposed into a mean and fluctuating component, with the fluctuations decaying rapidly toward zero. Moreover, the RANS equations provide reasonable results when interactions, separation, and recirculation are simple.

The continuity (1.a) and momentum (1.b) equations of the RANS averaged Navier-Stokes are as follows:

$$\begin{cases} \dfrac{\partial \bar{u}_i}{\partial x_i} = 0 \\ \dfrac{\partial}{\partial t}\left(\rho \bar{u}_i\right) + \dfrac{\partial}{\partial x_i}\left(\rho \bar{u}_i \bar{u}_j\right) = \rho f_i - \dfrac{\partial \bar{p}}{\partial x_i} + \dfrac{\partial}{\partial x_j}\left[\bar{\tau}_{ij} - \rho \overline{u_i' u_j'}\right] \end{cases} \quad \text{..... (1)}$$

Since there are more unknowns than equations, a strategy to "close" the system a is required [12-13]. The feasible k-ε closure model is accurate for studying the velocity distribution of turbulent flow through a curved channel, according to Shaheed et al. [14]. it captures rotation, vortices, strong curvature of the streamline and the unknown dissipation ε which incorporates the mean square fluctuation of the vorticity. In this feasible k-ε viscous model, Shih et al. [15] considered the eddy viscosity not as a constant, but as a function depending on the system rotational angular velocity, the mean strain and rotation rates, and the turbulence properties (ε and k).

The feasible k-ε closure model is estimated by two equations (2) and (3):

L'équation de transport de l'énergie cinétique turbulente (k) :

$$\frac{\partial}{\partial t}(\rho k) + \frac{\partial}{\partial x_j}\left(\rho k u_j\right) = \frac{\partial}{\partial x_j}\left[\left(\mu + \frac{\mu_t}{\sigma_k}\right)\frac{\partial k}{\partial x_j}\right] + P_k + P_b - \rho\varepsilon - Y_M \quad \text{..... (2)}$$

Where the physical quantities are: density (ρ), mean velocity component (u_j), molecular dynamic viscosity (μ), turbulent viscosity (μ_t), turbulent Prandtl number for k (σ_k), production of k due to shear (P_k), production of k due to buoyancy (P_b), dissipation rate of k (), contribution of expansion in compressible flows (Y_M).

The dissipation rate transport equation (Ɛ) :

$$\frac{\partial}{\partial t}(\rho\varepsilon) + \frac{\partial}{\partial x_j}\left(\rho\varepsilon u_j\right) = \frac{\partial}{\partial x_j}\left[\left(\mu + \frac{\mu_t}{\sigma_\varepsilon}\right)\frac{\partial \varepsilon}{\partial x_j}\right] + \rho C_1 S_\varepsilon - \rho C_{2\varepsilon}\frac{\varepsilon^2}{k + \sqrt{\nu_\varepsilon}} + C_{1\varepsilon}\frac{\varepsilon}{k}C_{3\varepsilon}P_b \text{ ..... (3)}$$

Where the physical quantities are: Turbulent Prandtl number for ε (σ_ε), strain rate modulus S,

$$S = \sqrt{2S_{ij}S_{ij}} \text{ avec } S_{ij} = \frac{1}{2}\left(\frac{\partial u_i}{\partial x_j} + \frac{\partial u_j}{\partial x_i}\right) \text{ et } \nu = \frac{\mu}{\rho}$$

Closure: turbulent viscosity

The turbulent viscosity is given by : $\mu_t = \rho C_\mu \dfrac{\kappa^2}{\varepsilon}$

$$C_1 = \max\left[0.43, \frac{\eta}{\eta+3}\right],\ \eta = S\frac{k}{\varepsilon}\ \ ,\ \ \tau_{ij} = -\frac{2}{3}\rho k\delta_{ij} + 2\mu_t S_{ij}$$

C_μ depends on the flow, it is not constant : $C_\mu = \dfrac{1}{A_0 + A_S\dfrac{k}{\varepsilon}s}$

With $A_0 = 4.04$ et $A_S = \sqrt{6}\cos\phi$, which depends on the local structure of the flow

$$\phi = \frac{1}{3}\cos^{-1}\left(\sqrt{6}\frac{S_{ij}S_{jk}S_{ki}}{\tilde{S}^3}\right);\ \tilde{S} = \sqrt{S_{ij}S_{ij}};\ C_\mu = 0.09;\ C_{1\varepsilon} = 1.44;\ C_{2\varepsilon} = 1.9;\ \sigma_k = 1.0;\ \sigma_\varepsilon = 1.2$$

The energy conservation equation can be expressed as follows: :

$$\frac{\partial T}{\partial t} + \frac{\partial}{\partial x_j}\left(T\bar{u}_j\right) = \frac{\partial}{\partial x_j}\left(\lambda_{eff}\frac{\partial T}{\partial x_j}\right) \qquad \text{..... (4)}$$

In Eq. (4):

T represents the temperature,

λ_{eff} is an effective coefficient that includes the contribution of turbulent mixing in addition to molecular conduction and can be expressed as: $\lambda_{eff} = \lambda + \dfrac{\mu_t Cp}{\mathrm{Pr}_t}$, where k and Cp are the thermal conductivity and specific heat at constant fluid pressure and μt is the turbulent viscosity.

Pr_t is a turbulent Prandtl number, we will take: Pr_t= 0.85.

3. Numerical Modeling and Validation:

Given the near impossibility of obtaining an exact analytical solution for the equations governing our problem, a numerical approach was favored. We used the finite volume method, renowned for its efficiency in terms of memory, computation time, and numerical stability, particularly when dealing with complex geometries [16]. For the discretization of convective terms, we selected the QUICK scheme, known for limiting numerical diffusion effects and offering high accuracy in capturing gradients [16]. This is particularly advantageous for turbulent flows or those with strong gradients. The pressure-velocity coupling was ensured using the coupled scheme. Numerical tests were conducted with rigorous convergence criteria set at 10^{-6} for the continuity, momentum, k-k, and energy equations to ensure accuracy, speed, and stability of the results. The mesh independence study was performed and found satisfactory. The numerical solution was performed using Ansys Fluent 2024R2 software.

Our results were validated through a satisfactory comparison with those of Wang Fuzhang et al. [11].

4. Analysis and discussion of results

Whether hot or cold, each inlet has its own characteristics (section, temperature and velocity, etc.), which implies distinct physical properties for each of the three inlets. These differences are reflected in particular by potential variations in quantities such as the mass flow rate and the total heat transfer rate for each inlet, which directly influences the flow dynamics and the heat transfer phenomena in the duct. Tables 2 and 3 present the mass flow rate and the total heat transfer rate for each inlet in each case for air and water.

Table 2 Mass flow rate [kg/s]

	Inlet 1 [kg/s]	**Inlet 2 [kg/s]**	**Inlet 3[kg/s]**
Motion of air	0.01539380400259	0.00461814120078	0.00461814120078
Motion of water	12.5437511472533	3.763125344176	3.763125344176

Table 3 Total heat transfer rate at the inlets [W]

	Inlet 1 [W]	**Inlet 2[W]**	**Inlet 3[W]**
Motion of air	77.4639308116332	-92.9567169739598	-92.9567169739598
Motion of water	78,686.9509467201	-1,049,159.34595627	-1,049,159.34595627

The meeting of the jets of the three inlets or addition of their physical quantities (mass flow rate or total heat transfer rate or momentum, etc. of each inlet) creates shocks or collisions at the mixing zone of the junction which will cause strong hydrodynamic and thermal interactions, disturbances and turbulence in the conduit. To establish and study its consequences, the velocity, temperature distribution and turbulent kinetic energy profiles in the (x,y,z=0) plane and at sections CS1 (i.e., the circular surface 30 mm after mixing), CS2 (i.e., another circular surface 100 mm from the mixing domain, before the first bend) and CS3 (i.e., the circular outlet surface, located 20 mm after the second bend of the duct) for different values of the length of the straight section connecting the two 90° elbowswith three cases: case I (L= 20 mm), case II (L=50 mm) and case III (L=100 mm) are presented according to the contours (Fig. 2-19).

We note that the mass flow rate of inlet 1 is greater than those of inlets 2 and 3. Despite this, at the intersection, the horizontal jet is disturbed by the two perpendicular jets from the two inlets (inlets 2 and 3). This causes a mixing zone, velocity gradients, and an increase in local velocity at the center of the junction. Flow acceleration is also observed after the junction (mixing zone) and before the first bend, following the radial direction, with the maximum velocity appearing at the duct axis (Fig. 2-7).

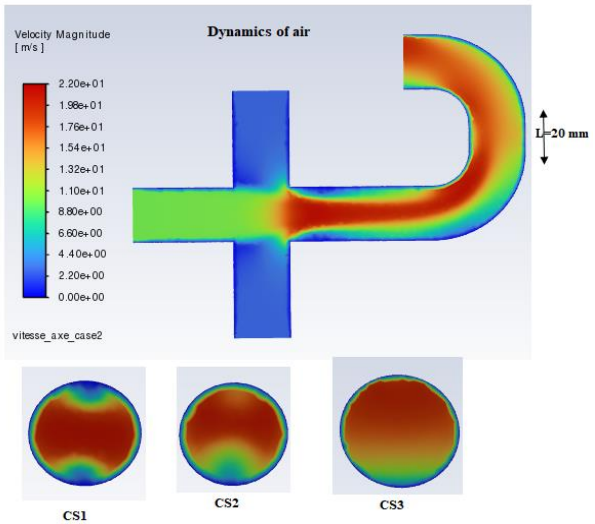

Figure 2 Velocity distribution across the domain of air dynamics - - Case I (*L*= 20 mm)

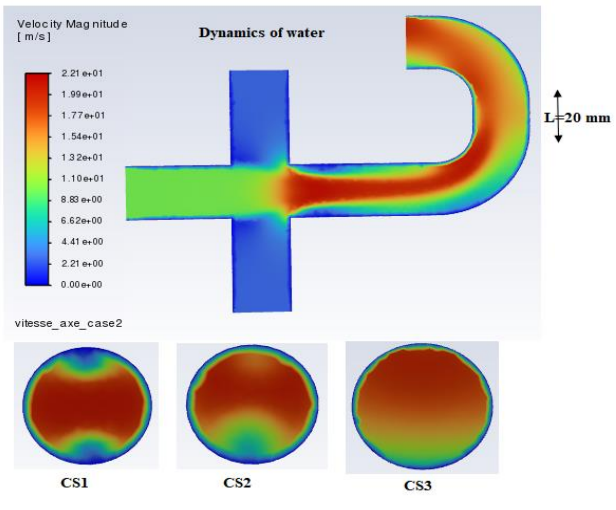

Figure 3 Velocity distribution across the domain of water dynamics - Case I (*L*= 20 mm)

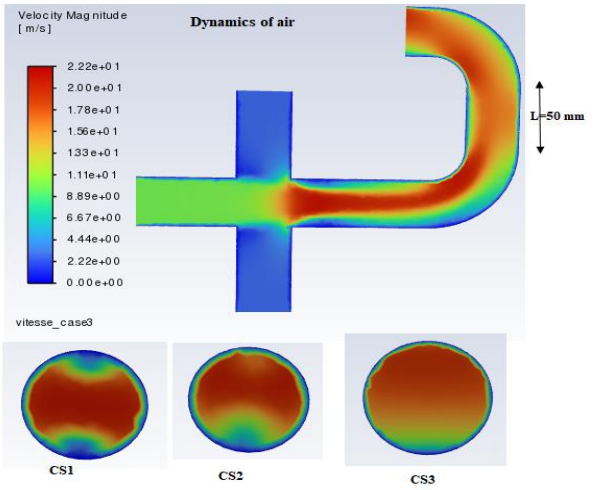

Figure 4 Velocity distribution across the domain of air dynamics - Case II (*L*= 50 mm)

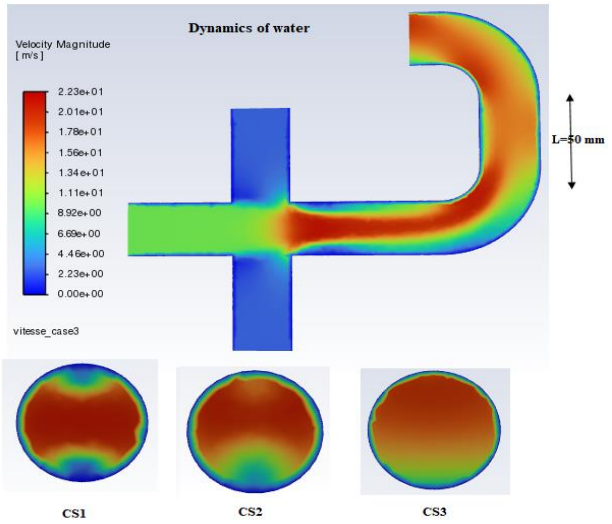

Figure 5 Velocity distribution across the domain of water dynamics - Case II (*L*= 50 mm)

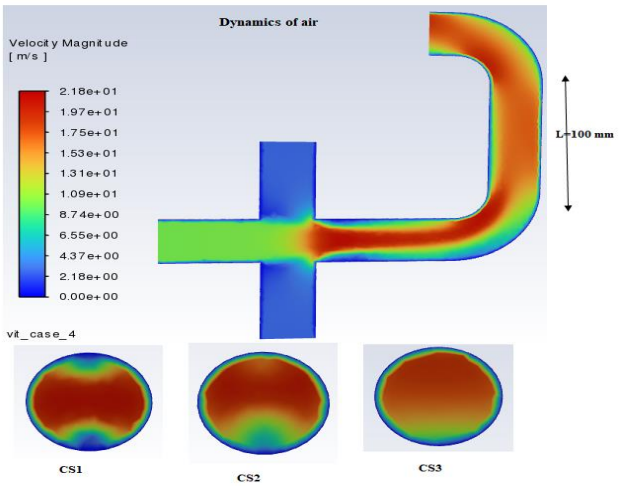

Figure 6 Velocity distribution across the domain of air dynamics - Case III (*L*= 100 mm)

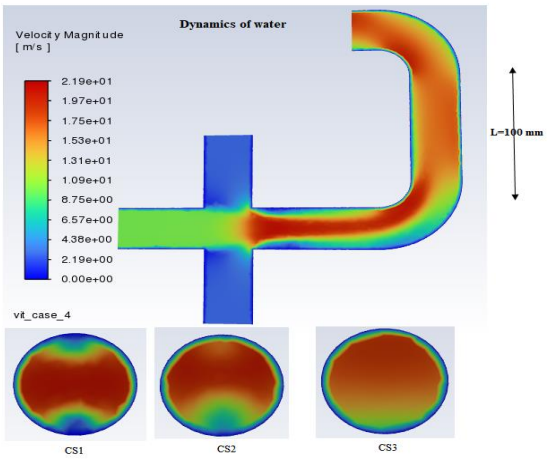

Figure 7 Velocity distribution across the domain of water dynamics - Case III (*L*= 100 mm

At the bends (in 'C', the two 90° elbows and the straight section), their centrifugal effects and secondary motions (Dean vortices) cause the peak velocity to be deflected toward the inner wall of the two bends. We observe that as the length of the straight section between the two bends increases, the velocity becomes more uniform in this zone, and its peak increases up to L = 50 mm and decreases thereafter. For example, for case I (L=20 mm), the speed can reach 22.0 m/s for air and 22.1 m/s for water; for case II (L=50 mm), the speed can reach 22.3 m/s for air and 23.2 m/s for water and finally for case III (L=100 mm), they fall and the maximum speed is 21.8 m/s for air and 21.9 m/s for water.

A sufficient straight section length allows for a restructuring of the velocity profile before the second bend (in the region between the two bends); extending this length is equivalent to softening the gradient. If the section is too short, the turbulent structures generated by the first bend can interact directly with the second bend, amplifying instabilities, and heterogeneous velocity zones are observed.

The length of the straight section acts as a buffer space for flow stabilization. It helps control the combined effects of successive bends on velocity. If it is too short, it aggravates disturbances; if properly dimensioned, it improves system performance.

Water velocities are higher than those of air due to its physical properties. The turbulent flow velocities of air and water through sections CS1 and CS2 appear to be nearly identical for Cases I (Fig. 2, 3), Case II (Fig. 4, 5), and Case III (Fig. 6, 7). In CS2 the effect of the first bend begins to be felt. In CS3, after the two bends the minimum velocity is rejected

towards the inner wall (blue spot at the bottom), a consequence of the superimposed recirculations of the fluid in the two bends (Dean vortex effect).

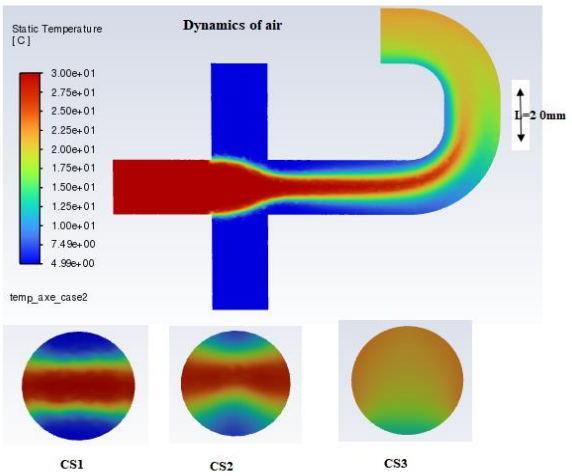

Figure 8 Temperature distribution across the domain of air dynamics - Case I (*L= 20 mm*).

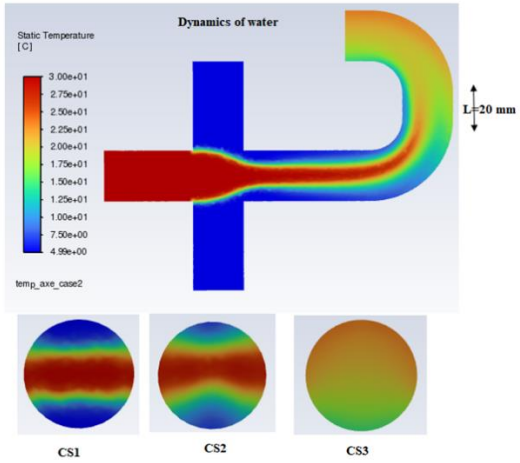

Figure 9 Temperature distribution across the domain of water dynamics - Case I (*L= 20 mm*).

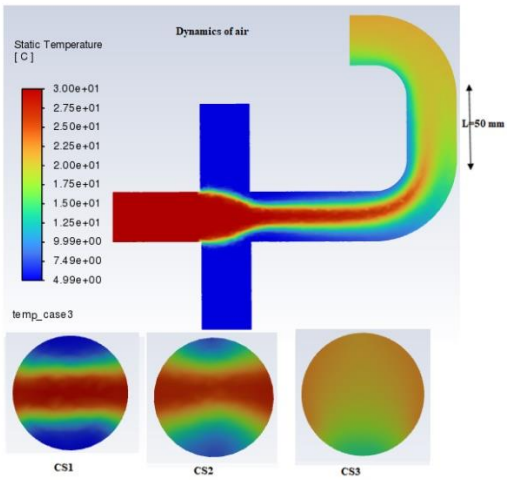

Figure 10 Temperature distribution across the domain of air dynamics - Case II (*L=50 mm*).

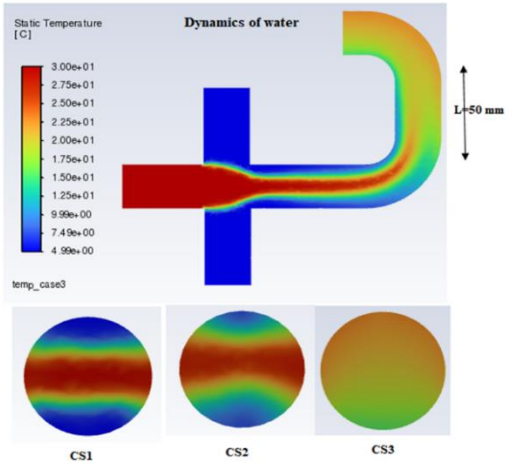

Figure 11 Temperature distribution across the domain of water dynamics - Case II (*L=50 mm*).

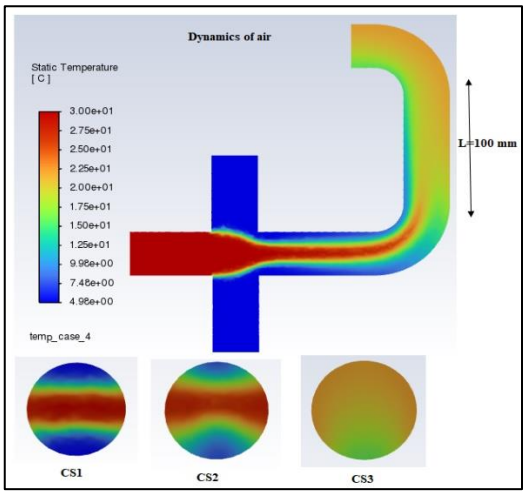

Figure 12 Temperature distribution across the domain of air dynamics - Case III (*L=100 mm*).

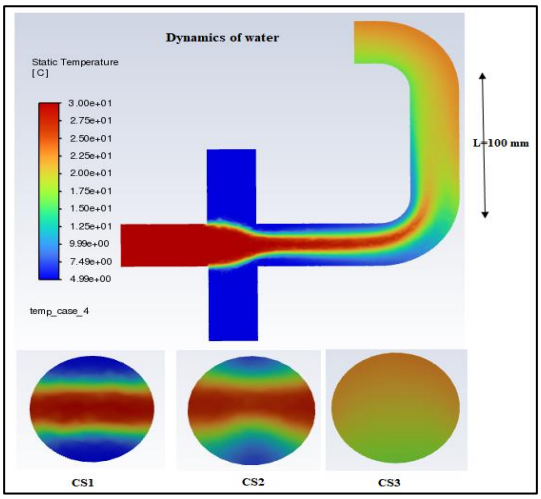

Figure 13 Temperature distribution across the domain of water dynamics - Case III (*L=100 mm*)

Fig. 8-13 shows the hot stream inlet 1 and the other two inlets (inlet 2 and inlet 3) that carry cold fluid. As the cold streams meet the hot stream, a sharp thermal transition zone called a cold front forms and emerges from the mixing zone of the junction along the duct axis.

This visible cold front formation is very important in the mixing domain. This is due to the significant changes observed in the temperature distribution with the velocities of each inlet.

The heat of the hot stream from inlet 1 is more dominant, so the temperature is little affected near the duct axis, even after the strong collision at the mixing zone. There is a dominance of hot air in the central zone, along the duct axis, and a gradual cooling in the lateral zones. The longer the straight section, the earlier and better the temperature homogenization in this region, the better the thermal mixing (especially if the fluid is conductive, like water) and the cold fronts are quickly dissipated there. While if the straight section is short, the temperature gradients remain intense due to the vortex structures, there is poor mixing and the recirculation zones can trap heat, promoting local thermal heterogeneities. We note that in CS2, the temperature is significantly more homogeneous than in CS1. The two bends triggered secondary flows (Dean vortex) which promoted optimal mixing in CS3.

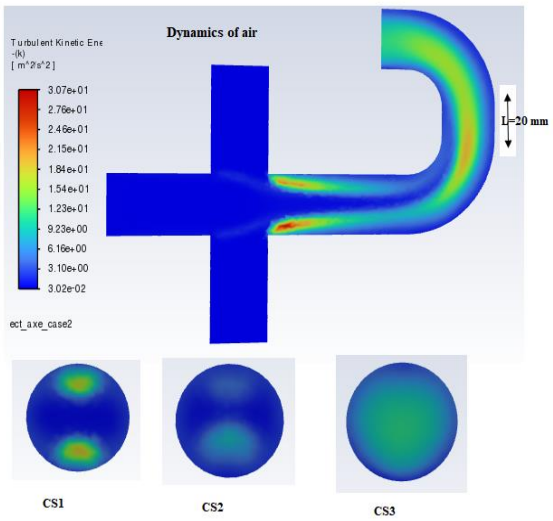

Figure 14 Turbulent kinetic energy across the domain of air dynamics - Case I (*L= 20 mm*).

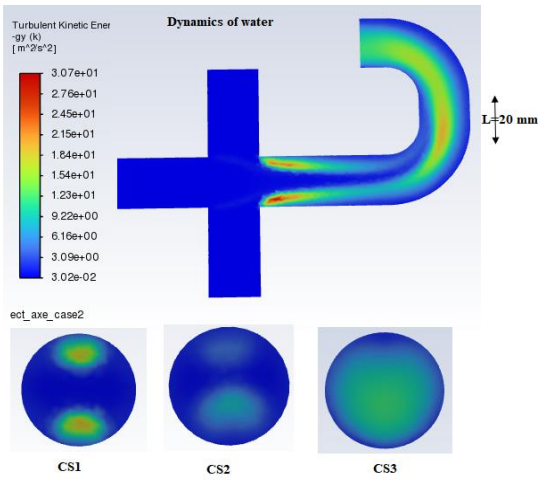

Figure 15 Turbulent kinetic energy across the domain of water dynamics - Case I (*L= 20 mm*).

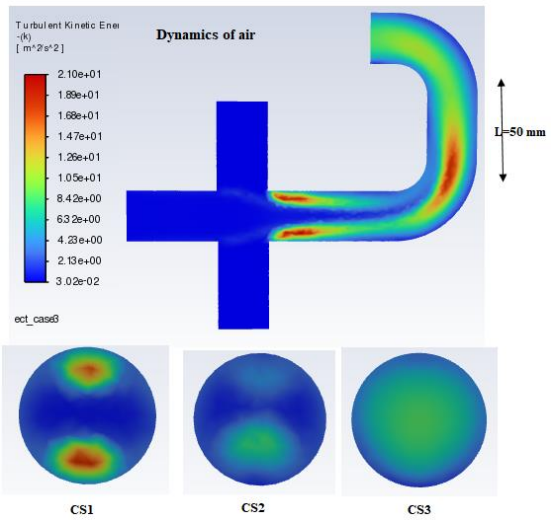

Figure 16 Turbulent kinetic energy across the domain of air dynamics - Case II (*L= 50 mm*).

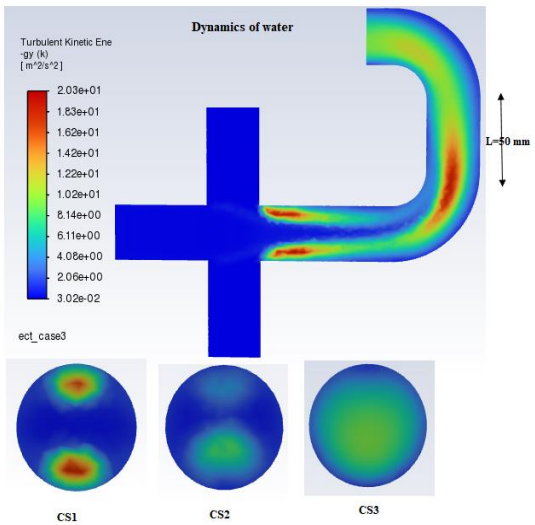

Figure 17 Turbulent kinetic energy across the domain of water dynamics - Case II (*L= 50 mm*).

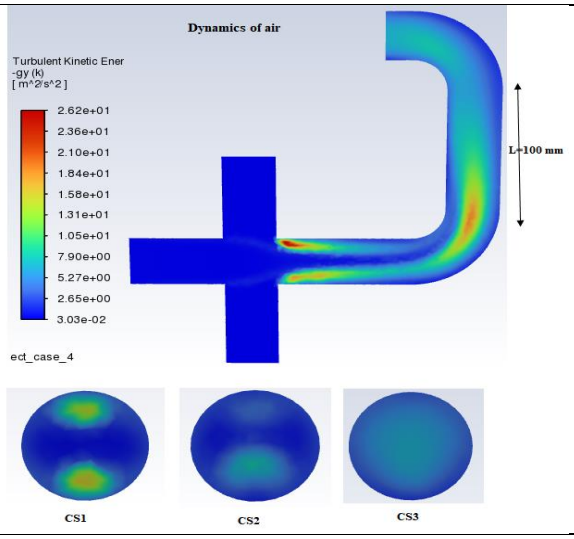

Figure 18 Turbulent kinetic energy across the domain of air dynamics - Case III (*L= 100 mm*).

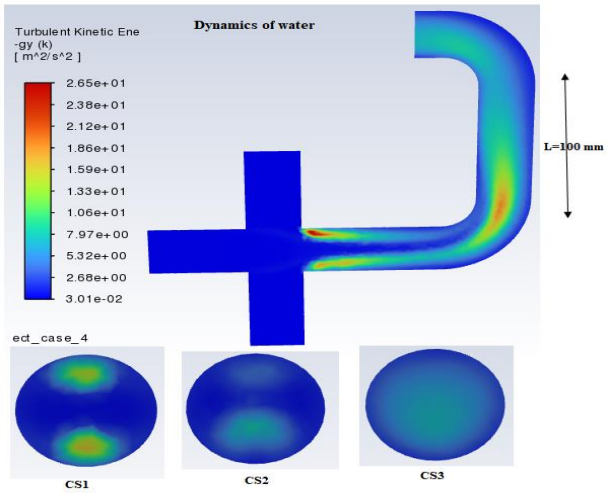

Figure 19 Turbulent kinetic energy across the domain of water dynamics - Case III (*L= 100 mm*).

The turbulent kinetic energy distribution contours are presented (Fig. 14-19). The latter evaluates the disorder of the local vortex motion and the intensity of turbulence in the flow. The zero turbulent kinetic energy at the three inlets implies a very ordered flow regime. It increases just after the mixing zone which is due to the interference of the jets from inlet 1 with inlets 2 and 3 at different speeds, creating strong velocity gradients and a high shear rate due to the perpendicularity of the jets. In the first elbow if the length of the straight section is short, the turbulent kinetic energy remains high because of the vortices inherited from the first bend, there are localized peaks of turbulent kinetic energy due to undissipated turbulent interactions. In the second bend and complete C bend, there is a superposition of the turbulent effects of the first and second bends, therefore a local increase in the turbulent kinetic energy can lead to additional losses and significant dynamic disorder. If the length of the straight section is long, the turbulent kinetic energy gradually decreases by turbulent diffusion and dissipation and the fluctuations become weaker and more homogeneous in the first bend. The turbulent kinetic energy remains controlled and its peak at the second bend is not aggravated by the turbulent residues of the first. The observation is very real that the water flows are more turbulent. This is mainly explained by its higher density and lower kinematic viscosity. The C-bend, consisting of two 90° elbows connected by the straight section, induces hydrodynamic disturbances as important but more diffuse and widespread than those observed with the T-junction with its peaks which are confined due to the perpendicularity and the direct and abrupt collisions of the flows in the mixing zone, which causes a lot of localized disturbances and increased and sharp turbulence. The C-bend acts as a turbulence amplifier in the conduit, with an intensity of the effects depending on the physical properties of the fluid (air and water) such as density and kinematic viscosity.

Nomenclature

Latin letters

- *Cp: Specific Heat, J/(Kg.K)*
- *D :* Main pipe diameter, m
- g : Acceleration of gravity, $m.s^{-2}$
- K: kinetic energy of turbulence, $m^2.s^{-2}$
- *P:* Pressure, Pa
- S_{ij} :Strain rate tensor
- *t* : Time, s
- $\overline{T}$: Filtered temperature, K^{-1}
- *u, v, w* : Velocity components, $m.s^{-1}$
- *u', v', w'*: Fluctuating velocity components, $m.s^{-1}$
- $\overline{u}_i$: Filtered velocity component in x_i direction, $m.s^{-1}$
- u_τ : Parietal Friction Velocity
- *x, y, z:* Cartesian coordinates, m
- *Pr:* Laminar Prandtl number

- Pr_t: Turbulent Prandtl number

Greek letters

- α : Thermal diffusivity, $m^2.s^{-1}$
- β: Coefficient of thermal expansion, K^{-1}
- λ: Thermal conductivity, $W.m^{-1}.K^{-1}$
- υ: Kinematic viscosity, $m^2.s^{-1}$
- ρ: Density, $kg.m^{-3}$
- μ: Dynamic viscosity, $kg.m^{-1}.s^{-1}$
- α : Thermal diffusivity, $m^2.s^{-1}$
- ν : Kinematic viscosity, $m^2.s^{-1}$
- σ_{ij}: Laminar stress tensor, Pa
- τ_{ij}: Subgrid scale stress tensor, Pa
- μ: Molecular dynamic viscosity, $kg.m^{-1}.s^{-1}$
- μ_t: Turbulent dynamic viscosity, $kg.m^{-1}.s^{-1}$
- ν: Molecular kinematic viscosity, $m^2.s^{-1}$
- ν_t: Turbulent kinematic viscosity, $m^2.s^{-1}$
- ε: Turbulence kinetic energy dissipation rate, $m^2.s^{-3}$

5. Conclusion

This paper investigated the air and water flows in a three-inlet T-junction duct followed by two 90° elbows connected by a straight section of adjustable length (C-shaped elbow). It focused on the impact of cold fronts, the fluid in question and especially the influence of the length of the straight section between the two 90° elbows. To achieve this objective, our analysis focused on the velocity, temperature distribution, and turbulent kinetic energy profiles in the (x,y,z=0) plane and at sections CS1 (i.e., the circular surface 30 mm after mixing), CS2 (i.e., another circular surface 100 mm from the mixing domain, before the first bend), and CS3 (i.e., the circular surface at the outlet of the duct, located 20 mm after the second bend) for different values of the length of the straight section connecting the two 90° elbows with three cases: case I (L= 20 mm), case II (L=50 mm), and case III (L=100 mm). The results showed us that:

- The length of the straight section acts as a buffer space for flow stabilization. It allows controlling the combined effects of successive bends on the velocity. Too short, it aggravates the disturbances; properly sized, it improves system performance.
- The length of the straight section between the two elbows plays a key role in the dissipation of dynamic disturbances, thermal rehomogenization, dissipation of cold fronts in the zone and reduction of turbulent kinetic energy. Too short, it promotes the amplification of thermal and hydrodynamic disturbances. Correctly dimensioned, it ensures better control of heat transfer and turbulence, with a direct impact on the thermo-hydraulic performance of the C-shaped elbow.
- The C-shaped elbow, consisting of two 90° elbows connected by the straight section, induces hydrodynamic disturbances that are as significant but more diffuse and widespread than those observed with the T-junction with its peaks that are confined due to the perpendicularity and direct and abrupt collisions of the flows in the mixing zone, which causes many localized disturbances and increased and sharp turbulence.
- The C-bend can be considered as a turbulence amplifier in the duct, with the intensity of the effects depending on the physical properties of the fluid (air and water) such as density and kinematic viscosity.

The need for proper sizing of the straight section, which acts as a flow stabilization zone in the duct, is essential. It ensures better control of heat transfer and turbulence, with a direct impact on its thermo-hydraulic performance.

Compliance with ethical standards

Disclosure of conflict of interest

No conflict of interest to be disclosed.

References

[1] A.S Athulya, C. R. Miji, 'CFD modelling of multiphase flow through T junction', International Conference on Emerging Trends in Engineering, Science and Technology (ICETEST 2015), Procedia Technology 24, pp 325 – 331, 2016..

[2] Mr.G.B. Nimadge, Mr.S.V. Chopade, 'CFD analysis of flow through t-junction of pipe', International Research Journal of Engineering and Technology (IRJET) Volume:4 Issue:2, pp. 906-911, Feb-2017.

[3] W. Khan, A. K. Chandra, K. Kishor , S. Sachan, M. S. Alam, 'Slug formation mechanism for air–water system in T-junction microchannel: a numerical investigation', Chemical Papers, 72(11), 2921–2932, (2018). https://doi.org/10.1007/s11696-018-0522-7

[4] Y. Doroshenko, J. Doroshenko, V. Zapukhliak, L. Poberezhny, P. Maruschak, 'Modeling computational fluid dynamics of multiphase flows in elbow and t-junction of the main gas pipeline', TRANSPORT, Volume 34 Issue 1, pp. 19–29, 2019. https://doi.org/10.3846/transport.2019.7441

[5] A. M. RAID, CFD instraction guide to simulate two-phase flow separation in a vertical T-junction separator. International Journal of Advances in Science Engineering and Technology, Vol-7, Iss-2, Spl. Issue-1 May-2019.

[6] Chiriac Eugen, Diana Broboana, Marioara Avram, Corneliu Balan, 'Comparative numerical study between OpenFOAM and ANSYS Fluent in a Y-junction microchannel', The 11th International Symposium on Advanced Topics in Electrical Engineering', March 28-30, 2019 Bucharest, Romania.

[7] M. A. Makarem, M. R. Kiani, M. Farsi M. R. Rahimpour, 'CFD Simulation of CO2 Capture in a Microchannel by Aqueous Mixtures of MEA and [Bmim] BF4 Modified with TiO2 Nanoparticles', International Journal of Thermophysics, Vol. 42 no. 4, (2021). https://doi.org/10.1007/s10765-021-02812-1

[8] E. S. Taha, M. A. Abdulwahid, A. M. A. Morad, Q. A. Maatooq, Computational Fluid Dynamic Analysis of the Flow though T-junction and Venturi Meter. Conference Paper ·IMDC-IST 2021, September 07-09, Sakarya, Turkey, pp. 1-9, Sept. 2021. http://dx.doi.org/10.4108/eai.7-9-2021.2314880

[9] M. Said, N. N. Bouda, S. Harmand, 'Numerical investigation of flow patterns and plug hydrodynamics in a 3D T-junction Microchannel', Research Square 2022. DOI:https://doi.org/10.21203/rs.3.rs-1613765/v1

[10] B. Khatoon, S. Ul Hasan, M. S. Alam, 'CO2 capturing in cross T-junction microchannel using numerical and experimental approach', Chemical Papers.- 77, pp. 6319–6340, July 2023. https://doi.org/10.1007/s11696-023-02941-x

[11] F. Wang, I. L. Animasaun, Q. M. Al-Mdallal, S. Saranya, T. Muhammad, 'Dynamics through three-inlets of t-shaped ducts: Significance of inlet velocity on transient air and water experiencing cold fronts subject to turbulence', International Communications in Heat and Mass Transfer, Vol. 148 (2023) 107034. https://doi.org/10.1016/j.icheatmasstransfer.2023.107034

[12] P. T. Ndiaye & O. N. Thiam, 'Computational fluid dynamics analysis of the influence of velocity at inlet 2 on heat transfer and fluid flow in the mixing elbow', Journal of Scientific and Engineering Research, vol. 11 no. 2, pp. 93-101, 2024.

[13] P. T. Ndiaye & O. N. Thiam, 'Computational Fluid Dynamics Analysis of the Influence of Diameter at Inlet 2 on Heat Transfer and Fluid Flow in the Mixing Elbow'. Journal of Applied Physical Science International, vol. 15 no. 2, pp. 61–70. https://doi.org/10.56557/japsi/2023/v15i28552.

[14] R. Shaheed, A. Mohammadian, G. H. Kheirkhah, 'A comparison of standard k-e and realizable k-e turbulence models in curved and confluent channels, Environ', Fluid Mech, Vol. 19 no. 2, pp. 543–568, 2019. https://doi.org/10.1007/s10652-018-9637-1.

[15] T.-H. Shih, W.W. Liou, A. Shabbir, Z. Yang, J. Zhu, 'A new k-ε eddy viscosity model for high Reynolds number turbulent flows', Comput. Fluids vol. 24 no. 3 pp. 227–238, 1995. https://doi.org/10.1016/0045-7930(94)00032-t.

[16] H. K. Versteeg, and W. Malalasekera, An Introduction to Computational Fluid Dynamics: The Finite Volume Method, 2nd ed. Harlow, England: Pearson Education, 2007.